2023-01-0516 Published 11 Apr 2023

Synthetic Grid Storage Duty Cycles for Second-Life Lithium-Ion Battery Experiments

Kevin Moy Stanford University

Simona Onori Stanford Univ

Citation: Moy, K. and Onori, S., "Synthetic Grid Storage Duty Cycles for Second-Life Lithium-Ion Battery Experiments," *SAE Int. J. Advances & Curr. Prac. in Mobility* 6(1):261-269, 2024, doi:10.4271/2023-01-0516.

This article was presented at the WCX SAE World Congress Experience, April 18-20, 2023.

Received: 03 Nov 2022 Revised: 09 Nov 2022 Accepted: 13 Dec 2022

Abstract

Lithium-ion batteries (LIBs) repurposed from retired electric vehicles (EVs) for grid-scale energy storage systems (ESSs) have the potential to contribute to a sustainable, low-carbon-emissions energy future. The economic and technological value of these "second-life" LIB ESSs must be evaluated based on their operation on the electric grid, which determines their aging trajectories. The battery research community needs experimental data to understand the operation of these batteries using laboratory experiments, yet there is a lack of work on experimental evaluation of second-life batteries. Previous studies in the literature use overly-simplistic duty cycling in order to age second-life batteries, which may not produce aging trajectories that are representative of grid-scale ESS operation. This mismatch may lead to inaccurate valuation of retired EV LIBs as a grid resource. This paper presents an end-to-end methodology that uses real-world electric grid power system data to simulate the cost-optimal dispatch for grid-scale ESSs. The dispatch is then used as an input to an algorithm which produces laboratory-prone, power-based synthetic duty cycles for second-life LIB cell aging experiments.

Introduction

Electric vehicles (EVs) are a key component of a low-carbon-emissions and sustainable transportation future. EVs are a rapidly-growing presence in transportation, from 120,000 vehicles in 2012 to over 6 million in 2021 worldwide [1]. The predominant EV energy storage technology used today is the lithium-ion battery (LIB). EV LIBs will degrade over time and with usage, due to the loss of lithium inventory, loss of active material, and formation of the solid-electrolyte interphase during cycling, manifesting as loss of usable capacity, an increase in internal resistance, and ultimately a reduction in usable energy and power from the device [2]. LIBs are retired from service in EVs when they can no longer provide satisfactory performance in EV operation. Retired EV LIBs could be repurposed as "second-life" energy storage systems (ESSs) for applications on the electric grid [3], supporting intermittent renewable energy production sources, such as solar photovoltaic (PV) and wind turbines, to meet the electricity load consumption as part of a low-carbon-emissions electric grid. After second-life usage, the LIBs can be disassembled and recycled into fresh LIB cells [4], forming a circular, low-waste economy for LIBs [5]. Both the demand for grid-scale ESS and the supply of retired EV LIBs for second-life will grow in scale, especially with wide-scale EV adoption and grid electrification. Second-life LIB supply is projected to be greater than 200MWh per year by 2030, rising to meet a projected 183MWh per year demand for grid-scale ESSs [6].

Second-life ESSs will behave differently from grid-scale ESSs constructed with fresh (unused) LIB cells due to the LIB degradation from first-life EV usage. In order to understand the degradation trajectory during second-life, laboratory experiments are used to age second-life LIB cells via duty cycles, which are current or power profiles representative of usage in a real application (in this paper, second-life ESS operation). For example, in [7], the capacity and power of second-life LIB cells were found to be much more sensitive to temperature changes than for first-life cells; furthermore, the distribution of cell capacities within a second-life pack showed a much greater spread than those in a fresh, first-life pack. In [8], second-life LIB cells with either lithium-iron phosphate (LFP) or blended nickel-manganese-cobalt/lithium-manganese-oxide (NMC-LMO) cathode chemistries were aged via dispatch (i.e., charging and discharging) corresponding to either either energy arbitrage or frequency regulation.

Many such studies in the literature use overly-simplified or *ad-hoc* selections of duty cycles. In [8], the energy arbitrage dispatch was simulated with a simple constant-current charge and discharge pattern, and the frequency regulation dispatch was chosen as a single day of a frequency regulation signal representing an entire year of operation, without justification. Similarly, the cells in [7] and in other studies [9, 10] were aged using constant-current/constant-voltage (CC/CV) cycles to simulate second-life operation. Namely, these laboratory experiments all use duty cycles based on current setpoints; in

field applications, the grid relies on constant power/energy requests from the ESS [11], which instead require power setpoints for the battery.

An important unanswered question for the deployment of second-life ESSs is the evaluation of their remaining economic and technological value, especially as fresh LIB cells continue to drop in price and other emerging technologies become more cost-competitive [3]. In contrast to the experimental second-life LIB aging literature, many studies using model-based simulations do use more realistic data to demonstrate the value of second-life ESSs. In [5], field data of load consumption and PV generation were used as inputs to simulate various second-life applications of EV LIBs, showing economic savings of 24% to 77%, depending on the scenario. In [12], energy market pricing signals from the China Southern Power Grid were used to simulate second-life ESS dispatch and the resulting LIB degradation, in order to provide a cost-benefit analysis and pricing plan for second-life LIB ESSs. In [13], the techno-economic benefits of second-life ESSs were evaluated using electricity pricing data from the California Independent System Operator and solar data obtained from the National Renewable Energy Laboratory, quantifying the economic value of second-life ESSs as <60% of their beginning-of-first-life price.

There is therefore a gap in data used by the literature for experimentally-aged cell datasets and for modelling and simulation of second-life LIB ESSs. In particular, by mitigating the mismatch between LIB aging datasets using simplistic duty cycles and second-life ESS economic valuation models, more accurate predictions/estimations of remaining economic value can be provided. In order to properly assess the value of second-life LIB ESSs, such models should be informed by application-dependent degradation data [14], especially as ill-informed synthetic duty cycles have been shown to produce degradation trajectories that are not representative of real-world operation [15, 16]. In turn, laboratory studies on LIB degradation in second-life grid-scale ESSs require duty cycles that are representative of grid-scale ESS usage. To this end, this paper provides a methodology for obtaining power-based synthetic duty cycles representing grid-scale ESS operation for usage in LIB cell laboratory cycling experiments, from readily-available and measurable electric grid power system operational data.

Notation

The following notation is used in this paper:

1. mod is the modulus operator, where a mod n returns the remainder of a divided by n. For example, 33 mod 24 = 9.
2. $\lceil\cdot\rceil$ is the ceiling operator, which rounds its argument up to the nearest integer. For example, $\left\lceil \frac{900}{3.2} \right\rceil = \lceil 281.25 \rceil = 282$.
3. max $\{\cdot\}$ is the maximum function. For example, for discrete set $q(t)$, $t = 1, 2, \ldots, T$, max $\{q(t)\} \geq q(t), \forall t \in [1, T]$. If the set $q(t)$ is non-negative, max $\{q(t)\}$ is equivalent to the L_∞ norm.

System Descriptions

This paper focuses on two systems: the first represents a residential power flow system, and the second represents a commercial power flow system. Both systems share the same general structure shown in Figure 1, comprising of an ESS of rated maximum power P_{ESS} and rated energy E_{ESS}, an optional solar PV array, a building or facility load, and the distribution grid. The purpose of each system is to use power supplied by the ESS, solar PV, and distribution grid to satisfy the load power demand at all times.

Figure 1 shows the flow of positive power in the direction of the arrows between different system components. These power flows are denoted by the origin and destination of the power, with the convention that the variable name is the origin of the power, with the subscript the destination of the power. For example, $g_l(t)$ is the power flowing from the distribution grid to the load, and pv_{ESS} is the power flowing from the solar PV array to the ESS.

These power flows can be aggregated into $c(t)$ and $d(t)$, representing ESS charge and discharge, respectively; solar PV generation $pv(t)$; load consumption $l(t)$; and grid power supply to the system $g(t)$, as labelled in Figure 1. The aggregated power flows are described as follows. First, the ESS is restricted only to discharge to supply the load

$$d(t) = ESS_l(t) \tag{1}$$

The ESS can charge from either the solar PV array or from the distribution grid

$$c(t) = pv_{ESS}(t) + g_{ESS}(t) \tag{2}$$

In the real system, the ESS cannot simultaneously charge and discharge. To prevent this behavior in the optimization problem, a binary variable $d_{bin}(t) \in \{0, 1\}$ is introduced, which is 1 when the ESS is discharging (and therefore not charging), and 0 when the ESS is charging. This is used in combination

FIGURE 1 System architecture as modelled in this paper for both the residential and commercial power flow systems. Arrows denote the flow of positive power. The colors denote the origin of the power: orange depicts power originating from the solar PV array, green depicts power originating from the ESS, and gray depicts power originating from the grid. Finally, the aggregated power flows $c(t)$, $d(t)$, $pv(t)$, $l(t)$, and $g(t)$ are labelled in white boxes.

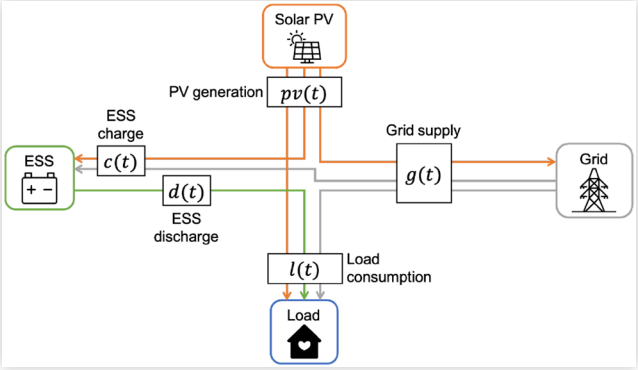

with P_{ESS} to constrain the dispatch within the physical operating limits of the ESS

$$d(t) \leq d_{bin}(t) P_{ESS} \tag{3}$$

$$c(t) \leq \left(1 - d_{bin}(t)\right) P_{ESS} \tag{4}$$

Next, the solar PV array can supply power to the ESS, the load, or back to the grid

$$pv(t) = pv_{ESS}(t) + pv_l(t) + pv_g(t) \tag{5}$$

Next, the grid supply is the net power supplied to the ESS and the load, minus the power backfed from the solar PV to the grid

$$g(t) = g_{ESS}(t) + g_l(t) - pv_g(t) \tag{6}$$

Finally, the load consumption is the sum of the power supplied from the grid, solar PV array, and the ESS

$$l(t) = g_l(t) + pv_l(t) + ESS_l(t) \tag{7}$$

$pv(t)$ and $l(t)$ are obtained from existing datasets as non-negative quantities (as described in the following subsections). This sets the sign convention of all other power flows: Power flowing from the solar PV array to other system components is non-negative, and power flowing from other system components to the load is also non-negative. For example, Equation 1 sets $d(t)$ as non-negative, as $ESS_l(t)$ is also a non-negative component of the load consumption as in Equation 7. Following this, all power flows as defined in the preceding equations (Equations 1-7) are non-negative

$$\begin{aligned} &c(t), d(t), pv(t), l(t), ESS_l(t), \\ &pv_{ESS}(t), pv_l(t), pv_g(t), g_{ESS}(t), g_l(t), \geq 0 \end{aligned} \tag{8}$$

Residential System

The residential ESS is modelled after a Tesla Powerwall, with P_{ESS} = 7kW and E_{ESS} = 13.5kWh [17], of which the minimum and maximum state of energy (SOE) is 20% and 80%, respectively. The load and PV data are obtained for a home in San Diego, California, USA from Pecan Street Inc. Dataport, which includes residential power flow data from several locations in the United States [18]. The load and PV data span one calendar year (January 1, 2015 to December 31, 2015). The tariff data are obtained from the San Diego Gas and Electric tariff for Schedule DR-SES, a time-of-use (TOU) rate without peak demand charges, used for residential customers with distributed energy resources such as solar PV and on-site ESS [19]. The residential power flow system dataset is shown in Figure 2 in the left-most column.

Commercial System

The commercial ESS is modelled after a Tesla Powerwall, with a maximum power of P_{ESS} = 200kW and rated usable energy of E_{ESS} = 800kWh [20]. As with the residential ESS, the commercial ESS minimum and maximum state of energy (SOE) is 20% and 80%, respectively. The load data are obtained for the Lawrence Berkeley National Laboratory Building 59 in Berkeley, California, USA, available on the United States Department of Energy's Benchmark Buildings Database [21]. This building does not report solar PV data, so the PV data for this system are set to 0 at all times (i.e. $pv(t) = 0, \forall t$). The load data span two calendar years (January 1, 2018 to December 31, 2019). The tariff data are obtained from the Pacific Gas and Electric tariff for Schedule B-10, a TOU rate with peak demand charges for commercial consumers without solar PV in the San Francisco Bay Area [22]. The specific tariff was selected based on the peak load demand ($\max\{l(t)\}$) of the facility. The commercial power flow system dataset is shown in Figure 3 in the left-most column.

Cost-Optimal ESS Dispatch

An optimization problem is formulated to simulate the cost-optimal ESS dispatch for each power flow system. The cost is the monthly utility bill, which is charged to the building owner based on the consumption of power from the grid $g(t)$ and determined by the utility tariff rate. The tariff rate comprises of two components: the TOU cost of energy at each time t, $C_E(t)$, in \$/kWh, and the demand charge for each month m, $C_P(m)$, in \$/kW. Altogether, the monthly utility bill J_m is

$$J_m = h \sum_{t=0}^{T_{m,h}} C_E(t) g(t) + C_P(m) \max\left\{g(t),\ t = 1,2,\ldots,T_{m,h}\right\} \tag{9}$$

where $T_{m,h}$ is the number of periods of length h hours in month m (e.g. in a month with 30 days, $T_{m,h} = 30 * 24 * 1/h$). In this paper, load and PV data are obtained at 15 minute intervals ($h = 0.25$).

The first term in the summation in Equation 9 represents the total cost of energy $C_E(t)$ consumed from the grid according to the TOU cost, and the second term represents the demand charge $C_P(m)$ applied to the maximum (peak) power consumed from the grid within the month.

The goal is to find the optimal charging $c*(t)$ and discharging $d*(t)$ profile of the ESS pack that minimizes the objective function J over the length of the entire load and PV dataset

$$J = \sum_{y=1}^{Y} \sum_{m=1}^{12} J_m \tag{10}$$

$$= \sum_{y=1}^{Y} \sum_{m=1}^{12} \left[h \sum_{t=0}^{T_{m,h}} C_E(t) g(t) + C_P(m) \max\left\{g(t), t = 1,2,\ldots,T_{m,h}\right\} \right] \tag{11}$$

where the total number of years Y is 1 for the residential system, and 2 for the commercial system. Next, the optimization constraints are formulated in terms of the ESS pack

FIGURE 2 Overview of all residential system data used and generated in this study. The first column contains the load, solar PV, and tariff rate data used to generate the cost-optimal ESS dispatch. The second column contains the cost-optimal dispatch and SOE. The third column contains the resulting residential synthetic duty cycle. The gray solid arrows depict the inputs and corresponding outputs of the optimization problem. The black dash-dot arrows depict the inputs and corresponding outputs of the synthetic duty cycle algorithm. In all plots, positive power corresponds to discharging.

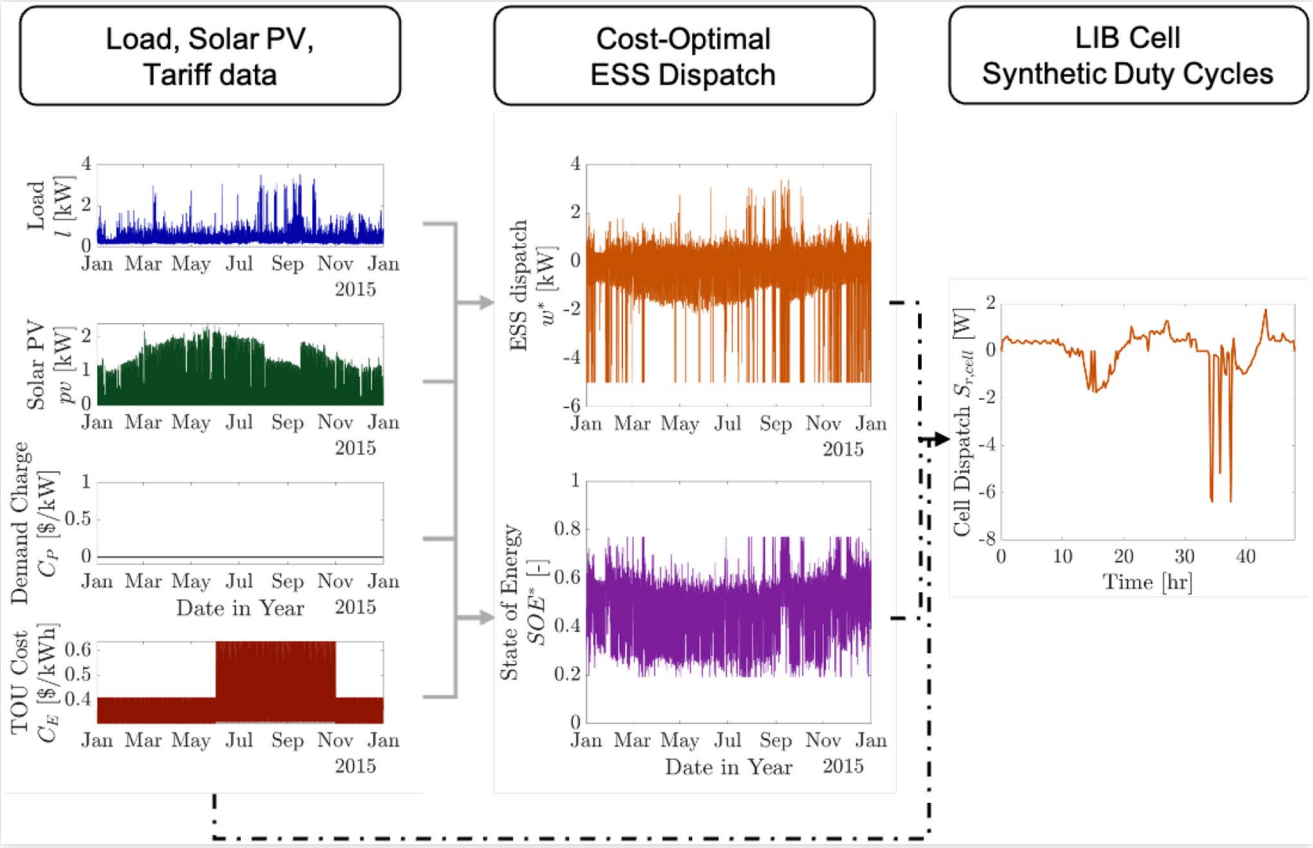

operational constraints and the power flows. The ESS pack is modelled as an energy reservoir where the control is the dispatch of the pack, while the state is the the stored energy $E(t) = SOE(t) * E_{ESS}$, governed by the following equation

$$E(t) = E(t-1) + h\left[c(t-1) + d(t-1)\right] \tag{12}$$

The stored energy is constrained so that it remains within the operational SOE limits of 20% and 80%

$$0.2E_{ESS} \le E(t) \le 0.8E_{ESS} \tag{13}$$

Additionally, the ESS pack is assumed to start and end each day at the same stored energy E_{init}, corresponding to SOE of 50% ($E_{init} = 0.5E_{ESS}$)

$$E\left(t : (ht+1) \bmod 24 = 0\right) = E_{init} \tag{14}$$

This constraint is introduced to facilitate the application of the synthetic duty cycle algorithm described in the next section. The ESS pack is also constrained to start and end each month at the same stored energy, also E_{init}

$$E(0) = E(T_{m,h}) = E_{init} \tag{15}$$

The ESS pack is also prohibited from charging or discharging at the end of the month

$$c(T_{m,h}) = d(T_{m,h}) = 0 \tag{16}$$

Equations 15 and 16 allow the monthly optimal dispatch to be solved separately, as the ESS starts and ends each month at the same state. Lastly, the system power flows are constrained by Equations 1-8 as defined in the "System Descriptions" section.

The optimal dispatch is the charge $c^*(t)$ and discharge $d^*(t)$ that satisfy the following

$$\min_{c,d} J$$
$$\text{Subject to Equations } 1-8 \text{ and } 12-16 \tag{17}$$

As constructed, this optimization problem forms a mixed-integer linear problem (MILP), consistent with other cost-optimal ESS dispatch in the literature [23, 24, 25]. The MILP is solved in Python using Gurobi, a solver for mathematical programming [26]. Along with $c^*(t)$ and $d^*(t)$, the resulting ESS state of energy $SOE^*(t)$ is returned as part of the solution to the MILP, and the cost-optimal dispatch $w^*(t)$ is computed as

$$w^*(t) = d^*(t) - c^*(t) \tag{18}$$

Following this sign convention, positive dispatch power corresponds to discharging, and negative dispatch power corresponds to charging.

FIGURE 3 Overview of all commercial system data used and generated in this study. The first column contains the load, solar PV, and tariff rate data used to generate the cost-optimal ESS dispatch. The second column contains the cost-optimal dispatch and SOE. The third column contains the resulting residential synthetic duty cycle. The gray solid arrows depict the inputs and corresponding outputs of the optimization problem. The black dash-dot arrows depict the inputs and corresponding outputs of the synthetic duty cycle algorithm. In all plots, positive power corresponds to discharging.

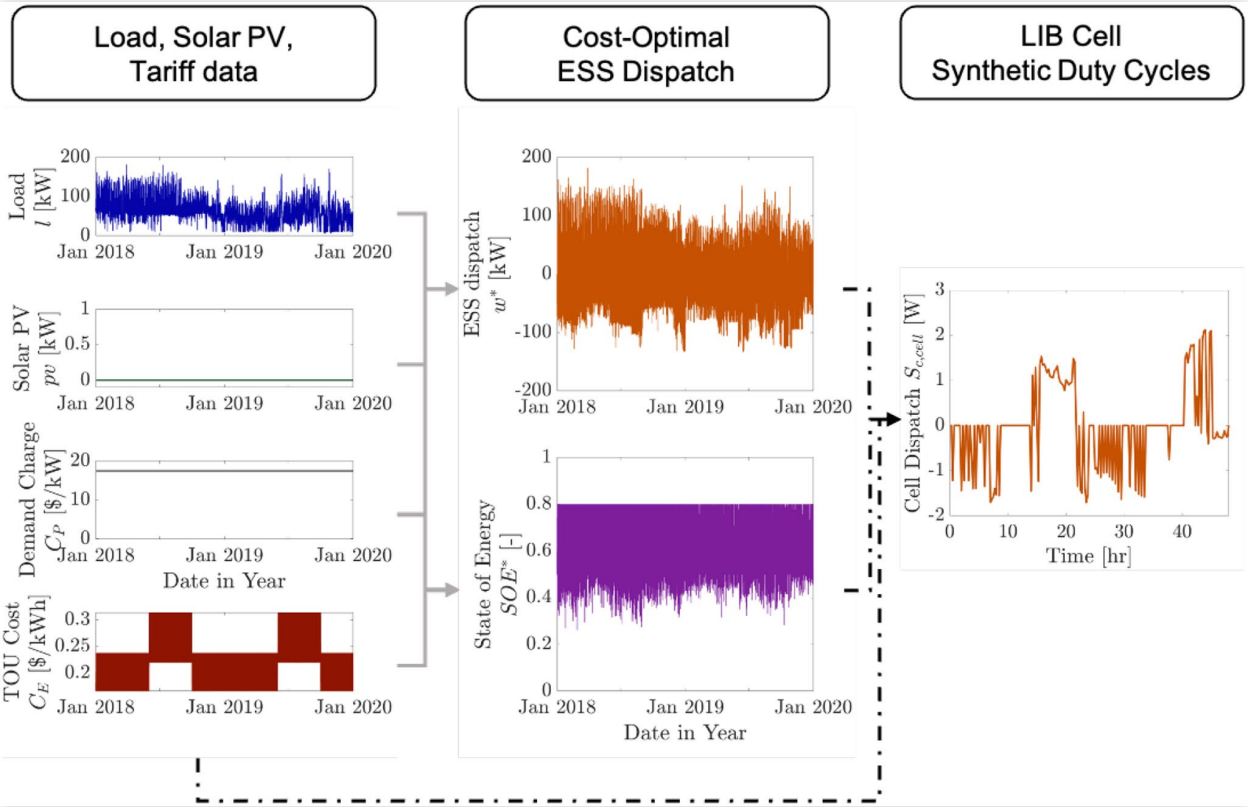

Synthetic Duty Cycle Formation

The synthetic duty cycle algorithm, previously published by the authors in [27] and summarized in Appendix B, is employed to create the grid storage synthetic duty cycles. The synthetic duty cycle algorithm is constructed and run in MATLAB. The algorithm takes the ESS state of energy $SOE^*(t)$ and power dispatch $w^*(t)$, along with time-of-use energy cost $C_E(t)$, as its input data. The algorithm then segments the inputs into "dispatch intervals"; as in [27], the dispatch intervals represent each 24-hour day of dispatch in the input data, starting at midnight. Therefore, the dispatch intervals are vectors of length $24 * 1/h$. A matrix is formed by computing metrics corresponding to different features of the dispatch (e.g., maximum discharge power) for each dispatch interval. Principal component analysis and k-means clustering are used to reduce the dimensionality of this matrix and select characteristic dispatch intervals, which are then concatenated to return the synthetic duty cycle $S(t)$ in terms of ESS power dispatch. In particular, Equation 14 ensures that each dispatch interval starts and ends with the ESS at the same state (SOE). This allows any dispatch intervals in the dataset to be concatenated together to form the synthetic duty cycle, without any discontinuity in the state of the ESS.

The LIB cells in the ESS are assumed to be identical NMC cells of nominal capacity $Q_{cell} = 4.85$ Ah and nominal voltage $V_{cell} = 3.63$V, with characteristics taken from [28]. As the cells are identical, the ESS power is divided by equally among its cells to produce the LIB cell power. In order to implement the synthetic duty cycles in LIB cell laboratory experiments, $S(t)$ must then be scaled down to the cell level. For this, the number of cells in series and in parallel are needed. The number of cells in series s are estimated as

$$s = \left\lceil \frac{V_{ESS}}{V_{cell}} \right\rceil \tag{19}$$

Where V_{ESS} is the nominal voltage of the ESS. Similarly, the number of cells in parallel p are estimated as

$$p = \left\lceil \frac{E_{ESS}}{V_{cell} Q_{cell}} \right\rceil \tag{20}$$

Then, given $S(t)$, the LIB cell synthetic duty cycle $S_{cell}(t)$ is

$$S_{cell}(t) = \frac{S(t)}{sp} = \frac{S(t)}{\left\lceil \frac{V_{ESS}}{V_{cell}} \right\rceil \left\lceil \frac{E_{ESS}}{V_{cell} Q_{cell}} \right\rceil} \tag{21}$$

For V_{ESS} of the residential and commercial ESSs, the Tesla Powerwall and Powerpack nominal voltages are used (V_{ESS} = 50V and V_{ESS} = 900V, respectively [17, 20]). From Equations 19 and 20, sp = 784 for the Tesla Powerwall, and for the Tesla Powerpack, sp = 47616. Therefore, for the residential and commercial synthetic duty cycles $S_r(t)$ and $S_c(t)$, $S_{r,cell}(t) = S_r(t)/784$ and $S_{c,cell}(t) = S_c(t)/47616$.

Results and Discussion

The residential and commercial synthetic duty cycles $S_{r,cell}(t)$ and $S_{c,cell}(t)$ are shown in the right-most column of Figures 2 and 3, respectively. The synthetic duty cycle algorithm selects representative intervals from the dispatch to form the synthetic duty cycles. Therefore, the corresponding SOE, tariff rate, and system power flows can also be obtained from the data for these synthetic duty cycles, representing the characteristics of ESS operation within each residential and commercial power flow system. These quantities are presented with the corresponding synthetic duty cycles in Figure 4 and 5, and provide a means to interpret the cost-optimal dispatch in each operation.

For example, in Figure 4, the commercial ESS charges from the grid in a fashion that limits the peak power demand from the grid, in order to reduce the demand charges. The ESS discharges predominantly when the tariff rate is higher in order to minimize the TOU cost, sometimes even matching the load consumption entirely so that grid supply is zero.

FIGURE 4 Clockwise from top-left: Commercial synthetic duty cycle (orange), with corresponding SOE (purple); demand charge (dark gray) and TOU cost (dark red); and system power flows: load consumption (blue solid line) and grid supply (gray dotted line). Note PV generated power is not plotted, as it os zero at all times for this dataset.

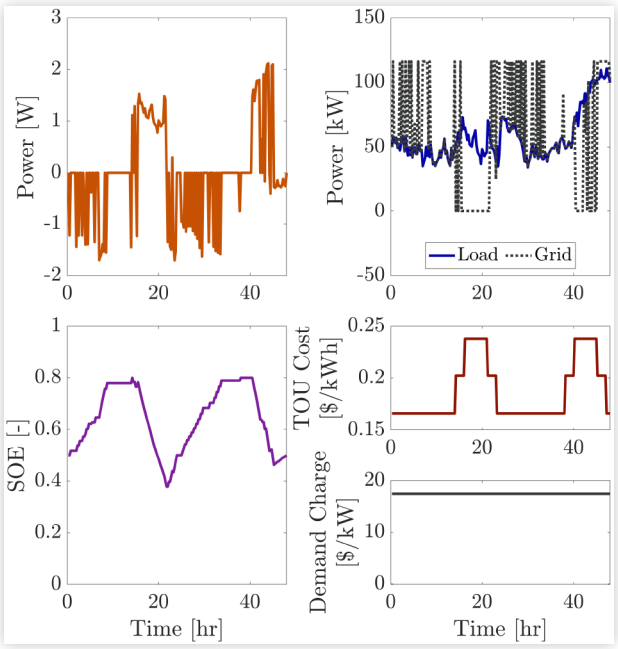

FIGURE 5 Clockwise from top-left: Residential synthetic duty cycle (orange), with corresponding SOE (purple); demand charge (dark gray) and TOU cost (dark red); and system power flows: load consumption (blue solid line), grid supply (gray dotted line), and PV generation (green dash-dot line).

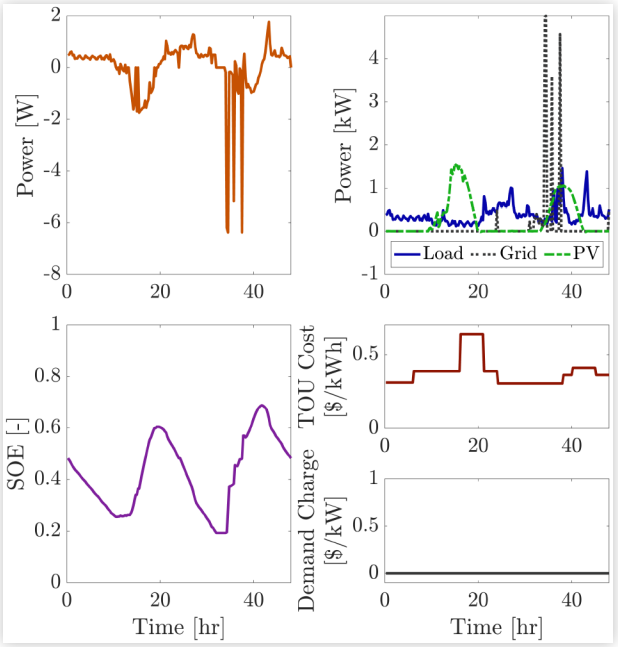

In contrast, in Figure 5, the residential ESS predominantly charges from PV generation, regardless of the tariff rate (as there is no cost to charge off of PV). In fact, the majority of the load consumption is either directly supplied by PV, or is supplied by ESS power stored from excess PV, resulting in a near net-zero flow of energy from the grid. During periods when the tariff rate is low and solar generation is low, the ESS is able to charge from the grid without any demand charges, as indicated by the spikes in grid power between hours 30 and 40. Finally, the stored energy constraints defined in Equations 13 and 14 are respected in both synthetic duty cycles: each cycle begins and ends at 50% SOE, and remains within the upper and lower bounds of 80% and 20% respectively.

Each synthetic duty cycle is also quantitatively compared to its originating cost-optimal dispatch via the synthetic duty cycle algorithm metrics in Table 1, shown in Figure 6. The synthetic duty cycles represent the cost-optimal dispatch along the majority of the metrics, but differ along others. In particular, the number of charge and discharge periods are much lower for the synthetic duty cycles compared to the entire dispatch, as expected given their highly-reduced length. The peak frequencies in charge and discharge also do not match between duty cycles and dispatch for the same reason; some of the transient components of the dispatch signals are lost when selecting a subset to form the synthetic duty cycles.

Finally, while the peak charging power matches well between the synthetic duty cycles and the entire dispatch, the synthetic duty cycle peak discharging power is lower than that of the entire dispatch.

TABLE 1 Summary of interval metrics used in the synthetic duty cycle algorithm in Algorithm 1.

Number	Name	Unit
1	Number of discharge periods	-
2	Number of charge periods	-
3	Peak discharge power	kW
4	Peak charge power	kW
5	Average discharge power	kW
6	Average charge power	kW
7	Average SOE in discharge	-
8	Average SOE in charge	-
9	Average tariff rate in discharge	$/kWh
10	Average tariff rate in charge	$/kWh
11	Peak frequency in discharge	Hz
12	Peak frequency in charge	Hz

FIGURE 6 Comparison between the input of the synthetic duty cycle algorithm (Residential Dataset, Commercial Dataset) to their corresponding outputs (Residential Synthetic Duty Cycle, Commercial Synthetic Duty Cycle), using the synthetic duty cycle metrics in Table 1. The x-axis is normalized to the maximum value for each metric.

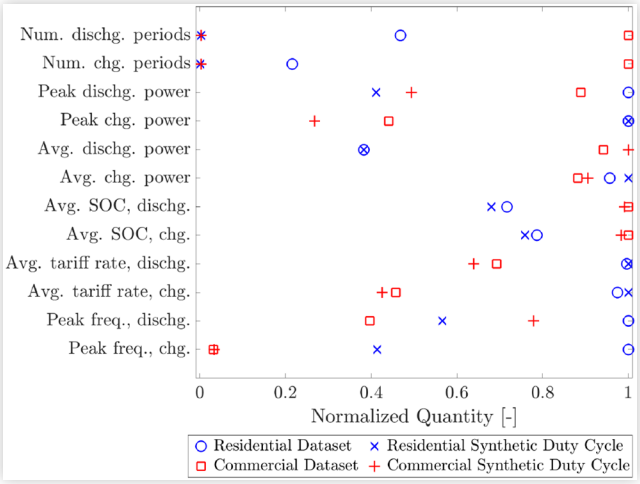

Summary/Conclusions

This paper presented an end-to-end methodology to produce laboratory-prone, power-based synthetic duty cycles for grid-scale ESS LIB cell experiments. These duty cycles were obtained from real-world power flow system data via a cost-optimal simulated ESS dispatch and an algorithm for synthesizing duty cycles. As the synthetic duty cycles are formed directly from characteristic intervals of the cost-optimal dispatch, this algorithm also enables the interpretation of the operational characteristics of ESSs in each grid application. The algorithm also provides a quantitative list of metrics to compare how well the synthetic duty cycles represent different characteristics of the dispatch. As more ESS operational field data are made available to the academic community, the synthetic duty cycle algorithm can be used to characterize real-world operation of ESSs and inform further laboratory experiments.

The synthetic duty cycles presented in this paper are currently being used to cycle the LIB cells presented in [28], which were aged using first-life EV driving cycles. The resulting dataset will form a second-life aging dataset, which can then be used to advance modelling and valuation of second-life LIBs for grid-scale ESSs.

References

1. International Energy Agency, "Global EV Outlook 2022," tech. rep., IEA, Paris, France, 2022, Available at https://www.iea.org/reports/global-ev-outlook-2022.
2. Shahjalal, M., Roy, P.K., Shams, T., Fly, A. et al., "A Review on Second-Life of Li-Ion Batteries: Prospects, Challenges, and Issues," *Energy* 241 (2022): 122881.
3. Zhu, J., Mathews, I., Ren, D., Li, W. et al., "End-of-Life or Second-Life Options for Retired Electric Vehicle Batteries," *Cell Reports Physical Science* 2, no. 8 (2021): 100537.
4. Chen, M., Ma, X., Chen, B., Arsenault, R. et al., "Recycling End-of-Life Electric Vehicle Lithium-Ion Batteries," *Joule* 3, no. 11 (2019): 2622-2646.
5. Thakur J., de Almeida C. Martins Leite, and Baskar A.G., "Electric Vehicle Batteries for a Circular Economy: Second Life Batteries as Residential Stationary Storage," *Journal of Cleaner Production*, vol. 375, p. 134066, 2022.
6. Engel, H., Hertzke, P., and Siccardo, G., "Second-Life EV Batteries: The Newest Value Pool in Energy Storage," April 2019, Available at https://www.mckinsey.com/industries/automotive-and-assembly/our-insights/second-life-ev-batteries-the-newest-value-pool-in-energy-storage.
7. Braco, E., Martín, I.S., Berrueta, A., Sanchis, P. et al., "Experimental Assessment of First- And Second-Life Electric Vehicle Batteries: Performance, Capacity Dispersion, and Aging," *IEEE Transactions on Industry Applications* 57, no. 4 (2021): 4107-4117.
8. Elliott, M., Swan, L.G., Dubarry, M., and Baure, G., "Degradation of Electric Vehicle Lithium-Ion Batteries in Electricity Grid Services," *Journal of Energy Storage* 32 (2020): 101873.
9. Liu, C., Wen, X., Zhong, J., Liu, W. et al., "Characterization of Aging Mechanisms and State of Health for Second-Life 21700 Ternary Lithium-Ion Battery," *Journal of Energy Storage* 55 (2022): 105511.
10. Ceraolo, M., Giglioli, R., Lutzemberger, G., Meskinfam Langroudi, M., Poli, D., Andrenacci, N., and Pasquali, M., "Experimental Analysis of NMC Lithium Cells Aging for Second Life Applications," in *2018 IEEE International Conference on Environment and Electrical Engineering and 2018 IEEE Industrial and Commercial Power Systems Europe (EEEIC/I&CPS Europe)*, 1-6, 2018.
11. Castillo, A. and Gayme, D.F., "Grid-Scale Energy Storage Applications in Renewable Energy Integration: A Survey," *Energy Conversion and Management* 87 (2014): 885-894.
12. Wu, W., Lin, B., Xie, C., Elliott, R.J. et al., "Does Energy Storage Provide a Profitable Second Life for Electric Vehicle Batteries?" *Energy Economics* 92 (2020): 105010.

13. Mathews, I., Xu, B., He, W., Barreto, V. et al., "Technoeconomic Model of Second-Life Batteries for Utility-Scale Solar Considering Calendar and Cycle Aging," *Applied Energy* 269 (2020): 115127.
14. Reniers, J., Mulder, G., and Howey, D., "Review and Performance Comparison of Mechanical-Chemical Degradation Models for Lithium-Ion Batteries," *Journal of The Electrochemical Society* 166 (2019): A3189-A3200.
15. Gong, H., Zou, Y., Yang, Q., Fan, J. et al., "Generation of a Driving Cycle for Battery Electric Vehicles: A Case Study of Beijing," *Energy* 150 (2018): 901-912.
16. Baure, G. and Dubarry, M., "Synthetic vs. Real Driving Cycles: A Comparison of Electric Vehicle Battery Degradation," *Batteries* 5, no. 2 (2019).
17. Tesla, "Tesla Powerwall," 2022, Available at https://www.tesla.com/powerwall.
18. Pecan Street Inc, "Pecan Street Dataport," 2020, Available at https://www.pecanstreet.org/dataport/.
19. San Diego Gas & Electric, "Time of Use (TOU) DR-SES," 2022, Available at https://www.sdge.com/regulatory-filing/2227/time-use-tou.
20. Tesla, "Tesla Powerpack," 2022, Available at https://www.tesla.com/commercial.
21. United States Department of Energy, Office of Energy Efficiency & Renewable Energy, "Benchmark Datasets for Buildings," 2022.
22. Pacific Gas & Electric, "Tariffs," 2022, Available at https://www.pge.com/tariffs/index.page.
23. Klaas, A.-K. and Beck, H.-P., "A MILP Model for Revenue Optimization of a Compressed Air Energy Storage Plant with Electrolysis," *Energies* 14, no. 20 (2021).
24. Moradzadeh, M. and Abdelaziz, M.M.A., "A New MILP Formulation for Renewables and Energy Storage Integration in Fast Charging Stations," *IEEE Transactions on Transportation Electrification* 6, no. 1 (2020): 181-198.
25. Hou, X., Wang, J., Huang, T., Wang, T. et al., "Smart Home Energy Management Optimization Method Considering Energy Storage and Electric Vehicle," *IEEE Access* 7 (2019): 144010-144020.
26. Gurobi Optimization, LLC, "Gurobi Optimizer Reference Manual," 2022, Available at https://www.gurobi.com.
27. Moy, K., Lee, S.B., Harris, S., and Onori, S., "Design and Validation of Synthetic Duty Cycles for Grid Energy Storage Dispatch Using Lithium-Ion Batteries," *Advances in Applied Energy* 4 (2021): 100065.
28. Pozzato, G., Allam, A., and Onori, S., "Lithium-Ion Battery Aging Dataset Based on Electric Vehicle Real-Driving Profiles," *Data in Brief* 41 (2022): 107995.
29. Moy, K., Lee, S.B., and Onori, S., "Characterization and Synthesis of Duty Cycles for Battery Energy Storage Used in Peak Shaving Dispatch," *ASME Letters in Dynamic Systems and Control* 1 (2021): 03.

Contact Information

Kevin Moy
kmoy14@stanford.edu

Simona Onori
sonori@stanford.edu

Acknowledgments

The research presented within this paper is supported by the Bits and Watts Initiative within the Precourt Institute for Energy at Stanford University and Chevron through the Stanford Chevron Fellowship in Energy.

Definitions, Acronyms, Abbreviations

CC - Constant current
CV - Constant voltage
EV - Electric vehicle
ESS - Energy storage system
LFP - Lithium-iron phosphate
LIB - Lithium-ion battery
LMO - Lithium manganese oxide
MILP - Mixed-integer linear problem
NMC - Nickel manganese cobalt
PV - Photovoltaic
TOU - Time-of-use

Appendix A: Nomenclature

Symbol	Unit	Quantity
P_{ESS}	kW	Rated maximum power of the ESS
E_{ESS}	kWh	Rated energy of the ESS
$c(t)$	kW	ESS charge power at time t
$d(t)$	kW	ESS discharge power at time t
$pv(t)$	kW	Solar PV power production at time t
$l(t)$	kW	Load power consumption at time t
$g(t)$	kW	Grid power supply at time t
$g_l(t)$	kW	Power flowing from grid to load at time t
$pv_{ESS}(t)$	kW	Power flowing from solar PV to ESS at time t
$pv_l(t)$	kW	Power flowing from solar PV to load at time t
$pv_g(t)$	kW	Power flowing from solar PV to grid at time t
$g_{ESS}(t)$	kW	Power flowing from grid to ESS at time t
$g_l(t)$	kW	Power flowing from grid to load at time t
$ESS_l(t)$	kW	Power flowing from ESS to load at time t
$C_E(t)$	$/kWh	TOU cost of energy for time t
$C_P(m)$	$/kW	Peak demand charge for month m
h	unitless	Temporal resolution of the data in fractions of an hour
$T_{m,h}$	unitless	Number of timesteps of the data at resolution h for month m
J_m	$	Monthly utility bill
Y	unitless	Number of years that the load and PV data span
$E(t)$	kWh	Stored energy in the ESS at time t

E_{init}	kWh	Initial stored energy of the ESS at the beginning of each day
$SOE(t)$	unitless	State of energy of the ESS at time t
$d_{bin}(t)$	unitless	Binary variable for ESS discharge
$c^*(t)$	kW	Optimal ESS charge at time t
$d^*(t)$	kW	Optimal ESS discharge at time t
$w^*(t)$	kW	Optimal ESS dispatch at time t
$S(t)$	kW	Synthetic duty cycle for the ESS at time t
s	unitless	Number of cells in series within the ESS
p	unitless	Number of cells in parallel within the ESS
$S_{cell}(t)$	W	Synthetic duty cycle for a single cell at time t
Q_{cell}	Ah	Nominal cell capacity
V_{cell}	V	Nominal cell voltage
V_{ESS}	V	Nominal voltage of the ESS
$S_r(t)$	kW	Residential synthetic duty cycle for the ESS at time t
$S_{r,cell}(t)$	W	Residential synthetic duty cycle for a single cell at time t
$S_c(t)$	kW	Commercial synthetic duty cycle for the ESS at time t
$S_{c,cell}(t)$	W	Commercial synthetic duty cycle for a single cell at time t
d	unitless	Interval used for synthetic duty cycle algorithm
D	unitless	Total number of intervals in the dataset
m	unitless	Number of metrics for dispatch metrics matrix
M	unitless	Interval metrics matrix
σ_i	unitless	Singular value i
v_i	unitless	Principal component i
p^*	unitless	Optimal number of principal components for dimensionality reduction
P	unitless	Reduced-dimension matrix representation of M
N_c	unitless	Optimal number of clusters for *k-means* clustering
k	unitless	Number of clusters used in *k-means* clustering
c_j	unitless	Cluster centroid j
r_j	kW	ESS power dispatch for representative interval j

Appendix B

The synthetic duty cycle algorithm is based on previous work from the authors [27], and is summarized in Algorithm 1.

ALGORITHM 1 Synthetic duty cycle algorithm

Require: Set of cost-optimal ESS dispatch power w^* and state of energy SOE^*, and tariff rate C_E, divided into D dispatch intervals

1: **for** $d = 1, 2, \ldots, D$ for D dispatch intervals **do**

2: Compute all m metrics for interval d using its corresponding dispatch power, state of energy, and tariff rate w^*_d, SOE^*_d, and $C_{E,d}$

3: Store normalized metrics for interval d in the dispatch interval matrix M

4: **end for**

5: Obtain principal components $v_1, \ldots, v_m$ and singular value $\sigma_1, \ldots, \sigma_m$ of M via PCA

6: Select number of principal components $p^* \in [1, m]$ as the minimum number of components needed to preserve 90% of the variance in the rows of M

7: Obtain PCA subspace matrix $P = M[v_1, v_2, \ldots, v_{p*}]$

8: Select optimal number of clusters, N_c to minimize intra-cluster distance and maximize inter-cluster distance

9: Obtain cluster centroids $c_1, c_2, \ldots, c_{Nc}$ of P with number of clusters N_c via *k-means* clustering

10: **for** $j = 1, 2, \ldots N_c$ **do**

11: Select representative interval d_j of cluster j as the cluster with smallest L2-distance to cluster centroid c_j

12: Obtain representative power interval dispatch $r_j = w^*_{d_j}$ as the characteristic duty cycle of cluster j

13: **end for**

14: Concatenate the N_c characteristic duty cycles to form the synthetic duty cycle $S = [r_1, r_2, \ldots, r_{Nc}]$

15: **return** Synthetic duty cycle S

The metrics computed for each interval (Line 2 of Algorithm 1) are shown in Table 1. Metrics relating to discharge are only computed in segments of the dispatch interval where power is non-negative (the "discharge periods"). Similarly, metrics relating to charge are only computed in segments of the dispatch interval where power is non-positive (the "charge periods"). The peak frequencies in charge and discharge are the peak of the power spectral density computed over the charge and discharge periods respectively, as computed in [29].

e-ISSN 2641-9645